Short-Range Energy-Aware Optical Wireless Communications Module for ns-3

Tiago Ribeiro, Sérgio Silva, João Pedro Loureiro, Eduardo Nuno Almeida, Nuno T. Almeida, Helder Fontes
INESC TEC and Faculdade de Engenharia, Universidade do Porto
Campus da FEUP, Rua Dr. Roberto Frias, 4200-465 Porto, Portugal
{tiago.s.ribeiro, sergio.m.marques, joao.p.loureiro, eduardo.n.almeida, nuno.t.almeida, helder.m.fontes}@inesctec.pt

***Abstract*—Optical Wireless Communications (OWC) has recently emerged as a viable alternative to radio-frequency technology, especially for the Internet of Things (IoT) domain. However, current simulation tools primarily focus on physical layer modelling, ignoring network-level issues and energy-constrained environments. This paper presents an energy-aware OWC module for ns-3 that addresses these limitations. The module includes specific PHY and MAC layers and integrates an energy model, a mobility model, and models of monochromatic transceivers and photodetectors, supporting both visible light and infrared (IR) communications. Verification against MATLAB simulations confirms the accuracy of our implementation. Additionally, mobility tests demonstrate that an energy-restricted end device transmitting via IR can maintain a stable connection with a gateway at distances up to $2.5\,\mathrm{m}$, provided the SNR is above $10\,\mathrm{dB}$. These results confirm the capabilities of our module and its potential to facilitate the development of energy-efficient OWC-based IoT systems.**

***Keywords*—OWC, IoT, ns-3, Energy-Aware, Short-Range**

I. Introduction

The Optical Wireless Communications (OWC) field is gaining significant attention as an alternative to traditional radio-based solutions due to its potential to address spectrum congestion, deliver higher data rates, and ensure secure communications [1]. This broad domain encompasses various technologies, including Visible Light Communications (VLC), infrared (IR), and Light Fidelity (Li-Fi). Moreover, OWC can complement other wireless communication solutions, such as Wi-Fi or Bluetooth Low Energy (BLE), making it a compelling option for the Internet of Things (IoT) domain [1]. Nevertheless, OWC requires extensive testing and simulation to realise its potential as an emergent technology. Current open-source OWC simulators primarily focus on modelling the physical (PHY) layer, while comprehensive network-level simulations are less common. For instance, [2] introduced an ns-3 module that combines VLC and Wi-Fi. However, this module derives from the point-to-point (P2P) module, which imposes significant limitations. In particular, the P2P module employs a simplified Medium Access Control (MAC) protocol designed for cabled communications and lacks a clear separation between the PHY and MAC layers. This design constraint prevents the implementation of energy models or targeted improvements to the PHY or MAC layers. In contrast, [3] developed a realistic VLC module with OMNeT++, which addresses these limitations by employing advanced ray-tracing techniques for channel modelling, providing dedicated PHY and MAC layers. However, although OMNeT++ is a simulation environment as capable as ns-3, only ns-3 allows for real-time integration with actual network stacks [4]. Lastly, none of these modules implements an energy consumption model for OWC. Therefore, developing a new energy-aware OWC module for ns-3 is worth exploring. This model would overcome the limitations of current solutions and facilitate the development of digital twins for energy-constrained OWC devices, ultimately advancing the practical deployment and optimisation of OWC technologies in energy-sensitive environments.

In this work, we present a novel OWC module for ns-3. The proposed OWC module focuses on modelling OWC in IoT networks, considering the nodes' mobility and energy consumption. For this purpose, we set up a scenario where the nodes are treated as IoT devices that operate on batteries and have energy harvesting capabilities. Therefore, we implemented an energy model that considers the energy consumed, stored, and harvested by the nodes. This scenario is characterised as a short-range communications environment, where nodes transmit through visible light (VL) and IR in distinct channels, enabling full-duplex communications. The OWC module is also designed with a modular architecture that enables reconfiguration and adaptation to user requirements, therefore broadening its potential applications and use cases. In this work, we explore the OWC module in an IoT context. Nevertheless, it can also be applied to other network architectures.

II. OWC Module Description

As mentioned, this work focuses on energy-restricted scenarios for IoT networks. Thus, the specifications were established in that context where, in each link, there is a central device and a peripheral one. Namely, the peripheral is designated as the end device (ED) and the central as the gateway (GW). The ED is energy-restricted, operating on batteries and relies solely on energy harvesting for its operation. Moreover, the GW is connected to the grid and has no energy limitations. The GW transmits via VL and receives via IR, whereas the ED operates oppositely, using IR for uplink (UL) and VL for downlink (DL). This configuration supports full-duplex communication, as the UL and DL occur on two different wavelength windows. Despite this full-duplex ability, devices of the same category (EDs or GWs) cannot communicate with each other because they transmit at wavelengths that they themselves cannot receive. This restriction imposes two main network topologies: a point-to-point link between ED and GW and a star network where the GW operates as the central node. Since this work focuses on IoT scenarios, these topologies are

perfectly aligned with the aimed goal.

In this module, the optical channel is defined within a narrow bandwidth instead of utilizing the full spectrum of a white LED. In this case, the LEDs are treated as monochromatic light sources, operating within a wavelength range of 1550 nm to 380 nm, covering both IR and VL. Both channels are modelled using the Lambertian propagation pattern, which is widely adopted for VL scenarios and can serve to model IR as well [5]. By treating IR and VL as monochromatic light sources and assigning the corresponding wavelengths to each, this simulator accounts for wavelength-dependent scenarios. Lastly, the Modulation Coding Scheme (MCS) employed is the Return-to-Zero On-Off Keying (RZ-OOK), chosen for its high energy efficiency and ease of implementation in modern LED technology [6]. A key reference for this work is [7], which provides a solid foundation in the fundamentals of OWC. In addition to theoretical insights, this reference includes MATLAB examples that were also utilized to validate our implementation.

A. Module Architecture

Fig. 1 depicts a high-level representation of this module architecture, showing the main building blocks of an OWC node. Each block represents a distinct class, following the typical architectural convention of an ns-3 module:

1) OwcNetDevice: This class abstracts and manages the network interface hardware. It handles tasks such as sending and receiving packets over the network, configuring network parameters, like IP addresses, and interfacing with the lower layers;

2) OwcPhy: This class is the first layer (physical) of the OSI Model. It is responsible for handling the physical transmission and reception of packets and also simulating errors that might occur during the transmission and reception of packets. This class integrates multiple components, such as an error model tailored for RZ-OOK and monochromatic optical transceiver and receiver models.

3) OwcMac: This class is responsible for the second layer (data-link) of the OSI Model. This class handles the protocols and mechanisms to control access to the shared wireless medium. The MAC follows a round-robin approach, where the GW cycles sequentially through each ED, which is particularly efficient for a star topology network. Additionally, the current MAC layer ensures a single connection between each unique pair of ED and GW while handling multiple connections from the GW side.

B. Optical Transceiver

In OWC, the transceiver usually consists of an array of multiple LEDs. However, in this module, the transceiver is a singular LED, representing the apparent luminosity of a combined grid. This device is modelled as a Lambert radiator, which can be configured with different parameters, such as the half power semi-angle $\phi_{1/2}$, the wavelength λ, the transmission power P_t, and the bit rate R_b. Depending on the configuration of the transceiver, this class is responsible for instantiating the *OwcSignalParameters* object, which encapsulates the data frame with the parametrization of the optical signal. The $\phi_{1/2}$ parameter represents the angle at which the luminous intensity decreases to half of its value along the central axis of the light's direction. Accordingly, the transceiver is then characterized by the Lambertian order, m, and the generalized Lambertian radiant intensity distribution, $R_0(\phi)$, defined as (1), where ϕ is the radiance angle, varying between $[-\pi/2, \pi/2]$ [7].

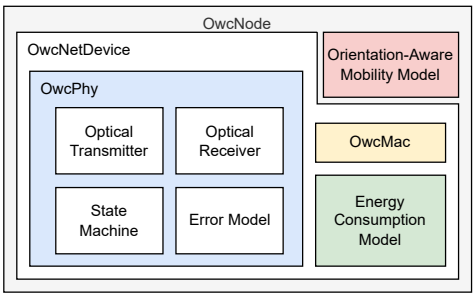

Fig. 1. High-level class diagram of the OWC ns-3 module.

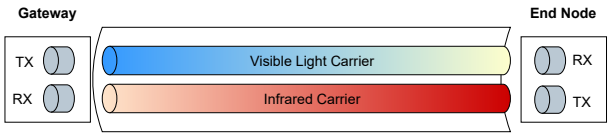

Fig. 2. Representation of the OWC channel.

$$R_0(\phi) = \frac{m+1}{2\pi}\cos^m\phi, \quad m = \frac{-\ln(2)}{\ln(\cos\phi_{1/2})} \tag{1}$$

C. Channel Model

The optical channel is implemented in the *OwcChannel* class. This class integrates the propagation loss and the propagation delay models while featuring VL and IR carriers, as shown in Fig. 2. In this model, each communication link between ED and GW is represented individually. This is possible since it is assumed that the medium access control is centralized at the GW. In fact, by cycling through each ED, the access control prevents collisions from happening. Consequently, there was no need to implement a collision resolution mechanism.

In OWC, two primary types of channels are the Line of Sight (LoS) link and the diffuse link [7]. This work adopts the LoS link for short-range scenarios. In this case, the multipath dispersion can be neglected. Thus, the LoS channel is often modelled as a linear system with attenuation and delay [8]. The optical LoS channels are regarded as non-frequency selective, with path loss inversely proportional to the square of the distance d between the transmitter and receiver. Indeed, the distance is one of the components of the channel's impulse response h_{LoS} as expressed in (2). Here $G_{pd}(\psi)$ represents the photodetector (PD) gain, given as (3), being ψ the incidence angle. $G_{pd}(\psi)$ is highly dependent on multiple parameters, such as the PD area A, the refractive index n, and the Field-of-View (FoV) angle ψ_c. Additionally, the concentrator gain $g(\psi)$ and the optical filter gain $T(\psi)$, are defined as (4) [7].

$$h_{\text{LoS}} = \frac{R_0(\phi)G_{pd}(\psi)}{d^2} \tag{2}$$

$$G_{pd}(\psi) = AT(\psi)g(\psi)\cos(\psi) \tag{3}$$

with $g(\psi)$ and $T(\psi)$ defined as:

$$g(\psi) = \begin{cases} \frac{n^2}{\sin^2(\psi_c)} & \psi \leq \psi_c \\ 0 & \psi > \psi_c \end{cases}, \quad T(\psi) = \begin{cases} T_s & \psi \leq \psi_c \\ 0 & \psi > \psi_c \end{cases} \tag{4}$$

D. Optical Receiver

The reception of the signal is handled by the *OwcPhotodetector* class, whose primary role is determining the SNR of the received signal as (5). This operation accounts for multiple parameters, combining the received power P_r, internal noise σ_n^2, and the photodetector's responsivity R. Moreover, the received power P_r is the product of P_t by the channel's impulse response h_{LoS}.

$$\text{SNR} = \frac{P_r R}{\sigma_n^2}, \quad P_r = P_t h_{\text{LoS}} \tag{5}$$

The responsivity R is given by (6), where q is the electron charge constant, h the Planck constant, c the constant speed of light in vacuum, and λ the wavelength of the received signal [9]. Additionally, quantum efficiency η represents the ratio at which a photon is converted to electrons upon receiving an optical signal. This value varies significantly depending on the photodetector's construction and varies non-linearly for different wavelengths. Thus, parameter η is a constant attribute that the user can configure to match the specs of the physical device.

$$R = \eta \frac{q\lambda}{hc} \tag{6}$$

Furthermore, total noise variance σ_n^2 is characterized by the sum of the thermal noise $\sigma_{\text{thermal}}^2$, and the shot noise σ_{shot}^2. The thermal noise is calculated as (7), based on the electronic characteristics of the PD. The shot noise, expressed as (8), depends on the wavelength and is caused by the arrival of the photons at the PD, modelling the noise interference from other light sources, such as ambient light [2]. Table I describes the parameters involved in this calculation.

$$\sigma_{\text{thermal}}^2 = \frac{8\pi k T_k C_{pd} A I_2 B_{eq}^2}{G_{ol}} + \frac{16\pi^2 k T_k \Gamma C_{pd}^2 A^2 I_3 B_{eq}^3}{g_m} \tag{7}$$

$$\sigma_{\text{shot}}^2 = 2qB_{eq}(RP_r + I_B I_2) \tag{8}$$

E. Error Model

The *OwcErrorModel* class implements the error model, asserting whether a packet is corrupted during the transmission. This process involves the bit error rate (BER) computation for a given SNR. In addition, the BER calculation is performed based on the MCS in use, as different MCS schemes exhibit varying resistance to noise. This work focuses on RZ-OOK, but other schemes are also supported as they were initially implemented in [2]. Therefore, the other available types of modulation are: Variable Pulse Position and Pulse Amplitude

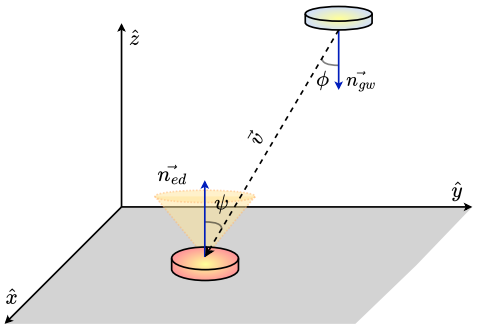

Fig. 3. 3D illustration of a gateway communicating with an end device.

for higher orders of modulation. For RZ-OOK, the BER is calculated as (9), and the Packet Error Rate (PER) as (10), where L represents the length of the received packet [6]. After computing the PER, the model determines whether a packet is corrupted by generating a random variable between 0 and 1. This value is then compared to the calculated value of PER. If the generated number is smaller than PER, the packet is corrupted; otherwise, the packet is delivered without errors.

$$\text{BER}_{\text{RZ-OOK}} = \frac{1}{2}\text{erfc}\left(\frac{\sqrt{\text{SNR}}}{2}\right) \tag{9}$$

$$\text{PER}_{\text{RZ-OOK}} = 1 - (1 - \text{BER}_{\text{RZ-OOK}})^{8L} \tag{10}$$

F. Orientation-Aware Mobility Model

Considering the calculations involved in modelling optical communications, the directionality and alignment between the nodes are important factors in the overall OWC model. Therefore, we developed a new mobility model that considers the orientation besides the (x, y, z) coordinates. This way, radiance and incidence angles are dynamically calculated based on the relative position of the nodes. The orientation is described by the surface's normal vector, with rectangular coordinates, on which the optical transmitter or receiver is installed. Thus, if multiple interfaces are installed on the same node, they share the same orientation.

Fig. 3 illustrates a scenario in which a GW is installed in the ceiling and communicates with an ED on the floor. The notation adopted describes $\vec{n_{ed}}$ and $\vec{n_{gw}}$ as the normal vectors to the surfaces of the ED and GW, respectively. The $\vec{v}$ represents the Line of Sight vector between them, and the ψ and ϕ angles are calculated as in (11). Additionally, the yellow-shaped cone represents the PD's FoV angle, meaning that if ψ is greater than ψ_c, the node is unable to receive the signal, becoming out of reach.

$$\psi = \arccos\left(\frac{\vec{n_{ed}} \cdot (-\vec{v})}{|\vec{v}|}\right), \quad \phi = \arccos\left(\frac{\vec{n_{gw}} \cdot \vec{v}}{|\vec{v}|}\right) \tag{11}$$

In addition to the mobility model, we created a helper class to handle its installation and configuration. This class allows users to define the room's dimensions, with the GW positioned at the ceiling's centre and the ED randomly distributed across the room floor. Additionally, the user can define the minimum

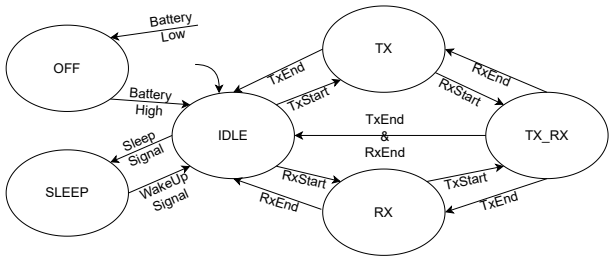

Fig. 4. OWC PHY state machine.

distance between EDs to avoid overlaps during random distribution. This helper class was mainly developed to facilitate the distribution of the nodes in a star topology network.

G. Energy Model

The energy model implemented utilizes the ns-3 energy framework [10]. In this framework, the energy model continuously monitors changes at the PHY layer and updates the energy consumption accordingly. This interaction between the energy model and the PHY layer requires three main components:

1) Energy Source Model: The energy source model represents a battery powering every component installed on a given node. Upon complete depletion, each interface gets notified and shuts down accordingly. Upon recharge, the interfaces are again notified and turned back on.

2) Energy Harvester Model: The energy harvester is natively supported in ns-3 and represents a photovoltaic cell as an energy source for the node.

3) Energy Consumption Model: This model computes the current draw according to the PHY state and time spent there. The user can instantiate two different models: the *OwcConstantCurrentModel* and the *OwcLinearCurrentModel*. The former acts as a look-up table, assigning fixed current draws to each state, regardless of the configuration parameters of the node. Conversely, the linear variation has the added functionality of calculating the TX current draw I_{tx} as (12), where P_t is the transmission power, V_s is the supply voltage, I_{idle} is the current in the idle state, and η_e is the power supply's efficiency, ranging between 0 and 1. These models were adapted from the Wi-Fi energy consumption model native to ns-3 [10] and are reconfigurable during runtime.

$$I_{tx} = \frac{P_t}{V_s \eta_e} + I_{idle} \tag{12}$$

The PHY layer has a state machine with six states, as illustrated in Fig. 4: Idle, Off, Sleep, Transmitting, Receiving, and Full-Duplex. As the node transitions between these states, the energy model is notified and updates the energy source according to the consumption model instantiated. Leakage current is also a configurable parameter of the simulation, and for this work it was set to 0 A.

III. Simulation Results

In this section, we evaluate the performance of the module in various scenarios. We verify the implementation of both the channel and mobility models and conduct experiments to evaluate the precision of the proposed energy models.

TABLE I. Simulation parameters for all scenarios

Parameter	Description	Value
P_{tx}	Transmission power	$1\,\mathrm{mW}$
R_b	Bit Rate	$1\,\mathrm{Mbit/s}$
$\phi_{1/2}$	Semi-angle	80°
η	Quantum efficiency	1
A	Area of the photodetector	$100\,\mathrm{mm}^2$
T_s	Filter gain	1
T_k	Absolute temperature	$295\,\mathrm{K}$
K	Boltzmann constant	$1.38 \times 10^{-23}\,\mathrm{J/K}$
ψ_c	FoV angle	70°
B_{eq}	Equivalent Noise Bandwidth	$4\,\mathrm{MHz}$
I_2	Noise bandwidth factors I_2	0.5620
I_3	Noise bandwidth factors I_3	0.0868
I_B	Background current	$1.13\,\mu\mathrm{A}$
G_{ol}	Open-loop voltage gain	10
C_{pd}	Fixed capacitance of the photodetector	$112\,\mathrm{pF/cm}^2$
Γ	FET channel noise factor	1.5
g_m	FET transconductance	$30\,\mathrm{mS}$
λ_{gw}	TX wavelength of the GW	$550\,\mathrm{nm}$
λ_{ed}	TX wavelength of the EDs	$1300\,\mathrm{nm}$
L	Packet size	39 Bytes
ns-3	ns-3 version	3.43

A. Validation Methodology

To evaluate the module's performance, we intend to confirm that the mathematical models selected from the literature were correctly implemented. Moreover, we aim to characterise the quality of the OWC link by analysing the SNR and packet loss under different conditions. In our validation, each scenario consists of a singular point-to-point link between the ED and the GW, consistent with a star topology. The round-robin scheduling ensures sequential communication without concurrency or collisions. Therefore, verifying each link independently allows us to isolate the core mechanisms while ensuring that the complete topology functions work as expected. Table I lists the default parameters across all scenarios, combining the transceiver and the PD configurations. The values regarding the noise characterisation in (7) and in (8) were adopted from [2], as the authors have tested their PD model in a real testbed. Other parameters, such as the transmission power P_t, bit rate R_b and packet size, were defined considering typical values in low-energy technologies such as in BLE [11]. For example, for the packet size, 39 bytes was chosen because it is the value of the BLE advertising protocol data unit, thus making it appropriate for low throughput IoT applications. In its turn, the RZ-OOK modulation requires a minimum bandwidth of $B_{eq} \geq 2R_b$ for a given bit rate R_b [6]. Thus, to achieve a maximum bit rate of $2\,\mathrm{Mbit/s}$, we defined the PD's equivalent noise bandwidth B_{eq} to $4\,\mathrm{MHz}$. Furthermore, the $\phi_{1/2}$ and ψ_c angles were selected to allow the gateway to fully cover the room. Finally, we compared the results obtained in ns-3 with the expected theoretical results from MATLAB simulations designed for each scenario.

B. Optical Link Validation

To evaluate the optical link performance, we designed a simulation scenario where the GW and ED face each other directly to determine the impact of the distance on the SNR. The GW was fixed in the ceiling at $(0, 0, 6)$, and the ED was placed underneath at $(0, 0, 6 - d)$, where d represents the distance between them. The ED starts at a close distance of

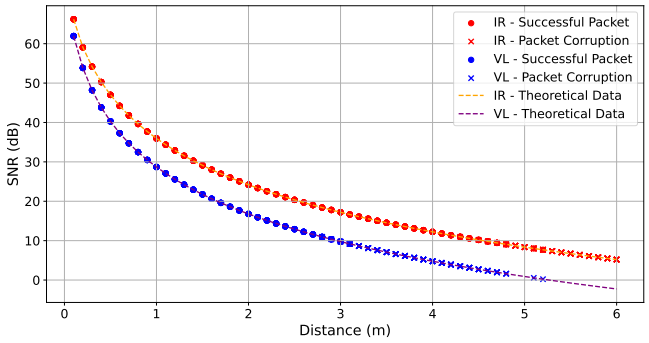

Fig. 5. SNR over the distance for IR and VL carriers, with markers for successful packet reception.

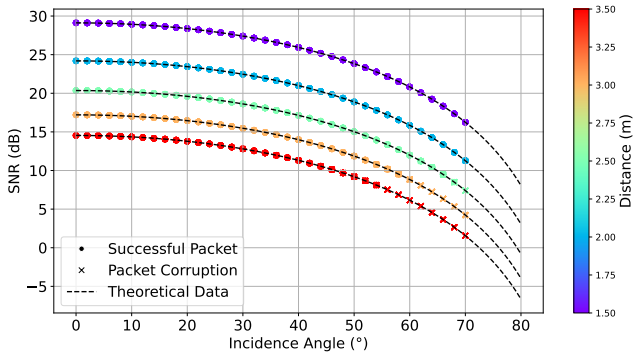

Fig. 6. Relation between the incidence angle, SNR and distance, with markers indicating packet reception successes and failures.

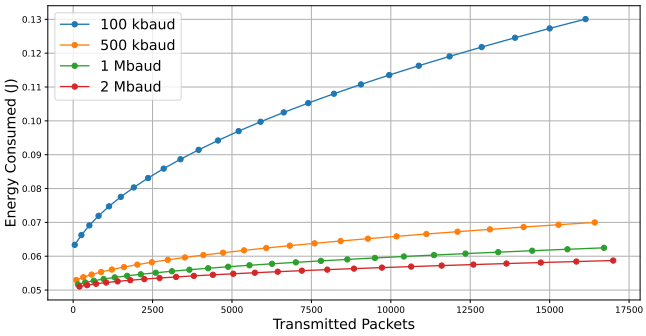

Fig. 7. Comparison of the total energy consumption depending on the baud rate and number of transmitted packets for a duration of 100 s.

0.1 m and gradually moves further apart up to a distance of 6 m. The GW receives IR signals, while the ED receives VL signals. We then collected SNR values from both devices and compared the performance of these two carriers under identical conditions. To validate our implementation, we developed a MATLAB simulation that calculates the theoretical SNR values over the distance, considering the same configuration parameters as in ns-3. As shown in Fig. 5, the values obtained in ns-3 match the theoretical calculations from MATLAB, confirming the module is correctly implemented. Additionally, we observe that IR communications outperform VL in terms of SNR. This is particularly useful as it allows using lower transmission power, making it more suitable for energy-constrained EDs. Furthermore, by distinguishing successful and unsuccessful connection events in our results, we observe that packet loss occurs when the SNR drops to around 10 dB, making the connection unreliable. This corresponds to a maximum distance of 4.3 m for IR, and 2.9 m for VL.

C. Mobility Tests

In this scenario, we evaluate the mobility of the ED within a room. We designed a setup where the GW remains fixed in the ceiling while the ED moves around it as in a pendulum motion. Initially, the ED faces the GW directly and gradually moves around it, covering its entire FoV. To further analyse the impact of distance, we repeated this experiment for various distances, varying it from 1.5 m up to 3.5 m, in increments of 0.5 m. The results, plotted in Fig. 6, include simulation results of this scenario and validation data from our MATLAB script. As with the previous scenario, the results align with the MATLAB calculations. Additionally, we can observe that the connection becomes unstable when the SNR drops to around 10 dB, regardless of the distance or incidence angle. The data shows that, for this configuration, the ED can maintain a reliable connection with the GW for a distance up to 2.5 m while being able to move freely within its FoV.

D. Energy Model

Regarding the energy-aware scenarios, we focused on verifying our implementation by observing that the energy consumption is simulated in coherence with the device's activity. At the current stage of development, the goal was not to validate the model's realism nor to optimize the node's energy consumption. We configured this scenario by installing the energy model on the ED with a fully charged battery. The current model was configured with $V_s = 3.3\,\mathrm{V}$, $\eta_e = 0.1$ and idle and RX current draws to 1.4 mA and 2.4 mA, respectively. These values were obtained from experimental measurements.

It is worth noting that in the idle state the node is only idle from a radio point of view. All systems are still powered up, ready to transmit and actively sensing, but the node is not actively transmitting. These parameters were adopted from the default values in the ns-3 Wi-Fi energy model using version 3.43.

1) Energy Consumption under different traffic loads: In this experiment, we defined a fixed simulation time of 100 s, placing the nodes at a distance of 1 m to avoid packet loss. For each simulation, we varied two key parameters: the baud rate of the ED and the total number of packets transmitted in this period. By adjusting the baud rate, we control how quickly each packet is transmitted. Conversely, by changing the number of transmitted packets during the same time interval, we control the traffic load of the connection. As illustrated in Fig. 7, higher baud rates result in less energy consumed for the same traffic load. This is justified because of the reduced time spent in the TX state, which results in a more efficient operation. However, our model does not account for the increased energy cost associated with the computational efforts of operating at higher baud rates. While this is a limitation, it also serves as a validation point, as the observed energy consumption trends confirm that the communication events are correctly reflected in the energy model.

2) Harvesting Scenario: In this scenario, we tested all components of the energy model by integrating an energy

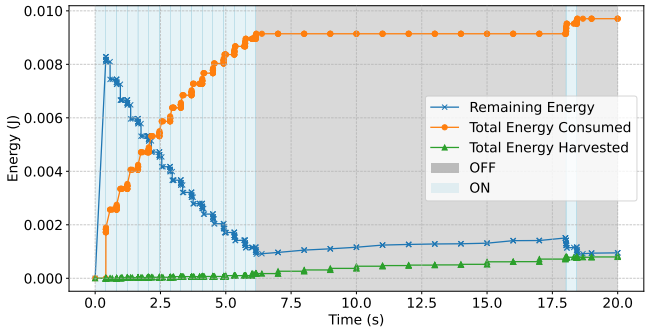

Fig. 8. Energy consumption, harvesting, and remaining energy over time. The blue background indicates the active state; the grey background indicates the harvesting state.

harvester in the ED. The goal is to observe the node depleting its battery, recharging, and correctly transitioning between on and off states. In addition, we wanted to ensure that communications are suspended during power loss and resume when sufficient energy is restored. To achieve this, we set up the simulation with trace-based data collection, where energy updates are logged whenever an event occurs. Specifically, whenever the node transmits or receives a packet or when it harvests energy, we capture the current remaining energy and update all relevant values. This approach allows us to monitor energy depletion and replenishment over time while providing insight into the node's activity. As shown in Fig. 8, we present three key metrics over time: the total energy consumed, the remaining energy in the node, and the harvested energy. Additionally, the graph background provides additional context, where blue regions indicate that the node is on and grey regions indicate the node is off. The simulation runs for $20\,\mathrm{s}$. The ED remains in operation during the first $6\,\mathrm{s}$, which is evident by the increased energy consumption. As the remaining energy reaches the lower threshold of $10\,\%$, the node shuts down, and the total energy consumed stabilizes, reflecting the absence of activity. During this period, the energy harvester continues to replenish the battery gradually. Eventually, the remaining energy reaches the upper threshold of $15\,\%$, allowing the node to resume operation briefly. However, because the available energy margin is small, the node quickly depletes its energy again and shuts down, repeating the cycle. This behaviour confirms that the energy model is correctly implemented, accounting for the communication dynamics.

IV. Conclusions

This paper presented a new ns-3 module for OWC, focusing on IoT networks. This work provides a coherent simulation environment with energy and mobility models and a PHY layer that integrates monochromatic transceiver and photodetector models. The results were aligned with the theoretical models, validating its implementation and precision. Furthermore, we analysed the performance of the optical link under low-power conditions. For our particular scenario, with a packet size of 39 Bytes and RZ-OOK, the link requires a minimum SNR of $10\,\mathrm{dB}$ to maintain a reliable connection. Moreover, the IR carrier proved to be more energy-efficient than VL. Transmitting with $1\,\mathrm{mW}$, the ED can maintain a stable connection with the GW within a range of $2.5\,\mathrm{m}$ without compromising its mobility. Finally, we demonstrated the behaviour of our energy model under different traffic loads, showing that higher baud rates lead to lower energy consumption of the ED due to the reduced time spent in the TX state. While this work provides a solid foundation, some limitations remain due to the lack of real-world data for validation. Future work will focus on improving the energy consumption model by conducting real-world experiments, adjusting the module's configuration parameters to match corresponding physical devices, as well as introducing more advanced OWC features such as beam pointing and steering. These improvements will enhance the module's realism and enable us to leverage machine learning techniques to optimise energy consumption. Beyond improving the module, we plan to integrate our OWC module into a real-world network, using emulated OWC nodes to scale real testbeds, bridging the gap between simulation and practical deployment.

Acknowledgements

The SUPERIOT project has received funding from the Smart Networks and Services Joint Undertaking (SNS JU) under the European Union's Horizon Europe research and innovation programme under Grant Agreement No 101096021, including top-up funding by UK Research and Innovation (UKRI) under the UK government's Horizon Europe funding guarantee.

References

[1] S. S. Oyewobi, K. Djouani, and A. M. Kurien, "Visible light communications for internet of things: Prospects and approaches, challenges, solutions and future directions," *Technologies*, vol. 10, 2 2022.

[2] A. Aldalbahi, M. Rahaim, A. Khreishah, M. Ayyash, and T. D. C. Little, "Visible light communication module: An open source extension to the ns3 network simulator with real system validation," *IEEE Access*, vol. 5, pp. 22 144–22 158, 2017.

[3] E. Torres-Zapata, V. Guerra, J. Rabadan, M. Luna-Rivera, and R. Perez-Jimenez, "MAC/PHY comprehensive visible light communication networks simulation," *Sensors*, vol. 20, no. 21, p. 6014, 2020.

[4] S. Manzoor, M. Manzoor, H. Manzoor, D. E. Adan, and M. A. Kayani, "Which simulator to choose for next generation wireless network simulations? ns-3 or OMNeT++," *Engineering Proceedings*, vol. 46, no. 1, p. 36, 2023.

[5] F. Miramirkhani and M. Uysal, "Channel modeling and characterization for visible light communications," *IEEE Photonics Journal*, vol. 7, no. 6, pp. 1–16, 2015.

[6] T. Y. Elganimi, "Performance comparison between OOK, PPM and PAM modulation schemes for free space optical (FSO) communication systems: Analytical study," *International Journal of Computer Applications*, vol. 79, no. 11, p. 22–27, 2013.

[7] Z. Ghassemlooy, W. Popoola, and S. Rajbhandari, *Optical Wireless Communications: System and Channel Modelling with MATLAB®*. CRC Press, 2019.

[8] S. Yahia, Y. Meraihi, A. Ramdane-Cherif, A. B. Gabis, D. Acheli, and H. Guan, "A survey of channel modeling techniques for visible light communications," *Journal of Network and Computer Applications*, vol. 194, p. 103206, 2021. [Online]. Available: https://www.sciencedirect.com/science/article/pii/S1084804521002101

[9] R. Paschotta, *Responsivity - Photodetectors, photodiodes, sensitivity*. RP Photonics AG, 2005.

[10] ns-3, "Energy framework," 2024, accessed: 2025-02-03. [Online]. Available: https://www.nsnam.org/docs/models/html/energy.html

[11] Bluetooth Special Interest Group, "Bluetooth core specification version 5.4," 2023, accessed: 2025-02-13. [Online]. Available: https://www.bluetooth.com/specifications/specs/core54-html/